Applied Catalysis B: Environmental 99 (2010) 74–80

Contents lists available at ScienceDirect

Applied Catalysis B: Environmental

journal homepage: www.elsevier.com/locate/apcatb

Photocatalytic oxidation of aqueous ammonia over platinized microwave-assisted titanate nanotubes

Hsin-Hung Ou[a,b], Michael R. Hoffmann[b], Ching-Hui Liao[a], Jian-Hao Hong[a], Shang-Lien Lo[a,*]

[a] Research Center for Environmental Pollution Prevention and Control Technology, Graduate Institute of Environmental Engineering, National Taiwan University 71 Chou-Shan Rd., Taipei 106, Taiwan
[b] W. M. Keck Laboratory, California Institute of Technology, Pasadena, CA 91125, USA

ARTICLE INFO

Article history:
Received 16 February 2010
Received in revised form 14 May 2010
Accepted 2 June 2010
Available online 12 June 2010

Keywords:
Photocatalysis
Aqueous ammonia
Platinized titanate nanotubes

ABSTRACT

Batch experiments were conducted to study the photocatalytic oxidation of aqueous ammonia (NH_3/NH_4^+) over platinized titanate nanotubes (platinized TNTs). The reaction kinetics of NH_3/NH_4^+ oxidation is considerably enhanced by the platinization of TNTs. The observed rate constant (k_{obs}) for NH_3/NH_4^+ oxidation over platinized TNTs was 1.69×10^{-2} min^{-1}, while the unamended TNTs gave a $k_{obs} = 1.23 \times 10^{-3}$ min^{-1}. The selectivity of nitrogen gas (N_2) from degraded NH_3/NH_4^+ increased with platinum loading to 87.8% after 1 h photocatalysis. In contrast, NH_3/NH_4^+ to nitrate (NO_3^-) conversion was low due to a large NH_3/NH_4^+ to nitrite (NO_2^-) energy barrier. High-resolution transmission electron microscopy shows that platinum deposits are formed primarily on the internal surface of the hollow structure of TNTs instead of being deposited on the external surface of TNTs. Based on the analysis of X-ray photoelectron spectroscopy, a mechanism is proposed in which N_2 is produced from the NH_3/NH_4^+ adsorbed on platinum deposits while NO_2^-/NO_3^- is formed from the NH_3/NH_4^+ adsorbed on titanate sites.

1. Introduction

Aqueous ammonia (NH_3/NH_4^+) is a major aquatic pollutant present in livestock waste. Both ammonium, NH_4^+, and its conjugate base, NH_3, are present in water [pK_a = 9.3 at 25 °C]. The presence of NH_3/NH_4^+ in natural water may cause eutrophication and enhance algal growth. High concentrations of NH_3/NH_4^+ in potable water may lead to the reduction in the efficiency of chlorine disinfection, the bacteria growth and the corrosion of copper pipes. Due to the acute toxicity of NH_3/NH_4^+, the maximum concentration of NH_3/NH_4^+ in potable water as set by World Health Organization is 1.24 ppm NH_3-N [1,2]. The current methods for removal of NH_3/NH_4^+ include breakpoint chlorination, ion exchange, air stripping, and biological nitrification and denitrification. In addition, the photocatalytic oxidation of NH_3/NH_4^+ over TiO_2 has also been proven to be effective treatment for NH_3/NH_4^+ control [1–5]. The effects of pH, initial concentration of NH_3/NH_4^+, and loading amounts of TiO_2 relative to the formation of nitrite (NO_2^-) and nitrate (NO_3^-) have been investigated [3,5–7]. However, few studies have focused on the selective formation of dinitrogen gas (N_2) during NH_3/NH_4^+ photooxidation. For example, Lee et al. [1] have shown that platinized TiO_2 enhances N_2 selectivity via the stabilization of NH_x, an intermediate leading to N_2. However, Pt oxides loaded on TiO_2 were shown to inhibit N_2 formation [2]. In another study, Nemoto et al. [8] reported that the H_2/N_2 molar ratio was about 3:1 in an Ar atmosphere. Pd supported TiO_2 also exhibited the ability to oxidize NH_3 to N_2 while Pt–TiO_2 under the same condition over-oxidized NH_3 to NO_x on the TiO_2 surface and NO_2^-/NO_3^- in aqueous solution [9].

Titanate nanotubes (TNTs) have several unique properties including large specific surface areas, significant photocatalytic ability, and distinct ion exchange capability [10–18]. However, there are conflicting reports in the literature that TNTs have superior photocatalytic activity compared to TiO_2 [12,13] whereas some studies show that TNTs are less photoactive [14,15]. In our previous studies, we synthesized TNTs ($Na_xH_{2-x}Ti_3O_7$) with the assistance of microwave irradiation and found that the intercalated amount of Na(I) within TNTs is enhanced with increasing power of the microwave irradiation [16]. We subsequently examined the photocatalytic oxidation of NH_3/NH_4^+ over TNTs and found that the light-shielding effect (filter effect), due to catalyst overloading is not apparent when NH_4^+ is intercalated into the zigzag structure of TNTs [17]. Efforts have also been focused on modifications to enhance the photoactivity of TNTs [19–21]. Nishijima et al. [19] modified S-doped TNTs with Fe_2O_3 nanoparticles and found that the visible light photoactivity was enhanced since the Fe_2O_3 loaded

* Corresponding author. Tel.: +886 2 23625373; fax: +886 2 23928830.
E-mail address: sllo@ntu.edu.tw (S.-L. Lo).

0926-3373/$ – see front matter © 2010 Elsevier B.V. All rights reserved.
doi:10.1016/j.apcatb.2010.06.002

on S-doped TNTs resulted in an efficient charge separation. A subsequent study reported improvements in visible light photoactivity by intercalating hetero metal ions into TNT structure [20]. Bouazza et al. report on the photocatalytic efficiency of propene oxidation over the hybrid material, carbon/titania nanotubes [21].

It is clear that transition metals can be intercalated into the hollow structure of TNTs [22–28]. However, few studies have examined the effects on photocatalytic performance.

In this paper, we synthesized platinized TNTs and investigated the photocatalytic oxidation of NH_3/NH_4^+. The kinetics of NH_3/NH_4^+ oxidation, the recoveries of NO_2^-/NO_3^- and the N_2 selectivity were examined. To clarify the effect of intercalated Pt on the NH_3/NH_4^+ photooxidation, major characterizations including UV–vis diffused reflectance spectroscopy (UV–DRS), X-ray powder diffraction (XRPD), and X-ray photoelectron spectroscopy (XPS) were also carried out to determine the surface features of platinized TNTs before and after photocatalytic reaction.

2. Experimental

2.1. Synthesis of unamended and platinized TNTs

The synthesis of TNTs was carried out using microwave hydrothermal methods, as we reported previously [16,17]. In a typical process, 70 mL of 10N NaOH solution along with 0.6 g of TiO_2 (Degussa P25) was treated at 130 °C for 3 h under the irradiation power of 100 W. After microwave hydrothermal treatment, the resulting precipitate was washed with 0.5N HCl repeatedly until the pH of suspension reached 7 ± 0.2. This neutralization process was followed by washing with 100 mL ultra pure water to remove excess NaCl. TNTs were subsequently dried using a vacuum freeze dryer for a minimum of 12 h (−58.8 °C and 100–200 mTorr).

The platinized TNT samples were prepared in the following way. 40 mL H_2PtCl_6 at a specific concentration was mixed with 1 g of TNTs in a 50 mL beaker. The slurry was stirred and heated in a water bath until it was thickened. After thickening the product was isolated again by drying with a vacuum freeze dryer for 24 h. To obtain the platinized TNTs, the resulting powders (H_2PtCl_6/TNTs) were then reduced under a gaseous mixture (20 vol.% H_2/80 vol.% N_2) at 350 °C for 2 h in a tubular furnace.

2.2. Kinetic procedures

The reaction of NH_3/NH_4^+ photooxidation was carried out in a well-mixed batch reactor. The cylindrical reactor was made of quartz with a capacity of 3 L, which is equipped with a double-walled cooling water jacket. A 400W UV medium-pressure Hg lamp with the emission wavelength larger than 254 nm (Philips Hok 4/120) was placed inside the cooling water jacket. The initial concentration of NH_3/NH_4^+ was prepared at 20 mg-N/L (5.9×10^{-4} M) in a 1.5 L slurry in which the unamended or platinized TNT samples were prepared at the concentration of 0.5 g/L. pH value was controlled at the range of 10 ± 0.2, since the oxidation rate of NH_3/NH_4^+ is very slow or negligible at pH values lower than 9 [3–6]. Air was continuously purged through the reactor during the course of the photolysis (6 h photoirradiation). At specific time intervals, sample aliquots of 5 mL were withdrawn from the reactor using a 10 mL syringe, and then filtered through a 0.22 μm filter (Milipore filter with 25 mm diameter and 0.2 mm pore size). The filtrates were collected with 10 mL glass vials, which were used for the measurements of NH_4^+/NH_3, NO_2^-, and NO_3^-. In a control experiment, less than 2% of NH_3/NH_4^+ was lost in the absence of UV light and catalyst. This indicated that the effect of air stripping was negligible during the time course of interest. The oxidation of NH_3/NH_4^+, therefore, can be attributed essentially to photocatalytic oxidation.

2.3. Analysis of NH_3/NH_4^+, NO_2^-, and NO_3^-

An ammonia gas-sensing electrode (model 95-12; Thermo Orion) connected to a model 720A+ Thermo Orion meter to determine the concentration of total ammonia. Before measurement, ionic strength adjustors (ISA, Thermo Orion) were added to the 10 mL standards and filtered samples to keep constant ionic strength and high pH value. The concentrations of NO_2^- and NO_3^- were measured by ion chromatography (Metrohm 790 personal IC), in which the detection limits for NO_2^- and NO_3^- were less than 0.1 mg/L. A mixed solution of 1.8 M Na_2CO_3/1.7 M $NaHCO_3$ was used as mobile phase, whose flow rate was controlled at 1 mL min^{-1}.

2.4. Determination of N_2 produced over unamended TNTs, 2 Pt wt%, and 20 Pt wt% TNTs

The produced amount of N_2 was determined by gas chromatograph/thermal conductor detector (GC/TCD; P5890) equipped with a 180 cm × 0.63 cm packed molecular sieve column (5 Å) using He as carrier gas. Regarding the determination of N_2 amount produced from photooxidation of NH_3/NH_4^+, a 15 mL vial made of quartz was prepared to be filled with 10 mL of 20 mg/L NH_3/NH_4^+ and 5 mg of TNT sample. After purging with air for 30 min, the vial was sealed with Teflon silicone septa and aluminum caps with the initial pH controlled at about 10 ± 0.2. The air in the headspace of vial was replaced by He repeatedly until a minimum amount of N_2 was achieved. The vial was subsequently exposed to UV light at ambient temperature. After 6 h photoirradiation, aqueous samples were filtered using a 0.22 μm filter and analyzed immediately. The analytic methods for NH_3/NH_4^+, NO_2^-, and NO_3^- were the same as the described above. Before sampling the aqueous products, the gaseous samples were withdrawn from the headspace of vial by a 50 μL syringe. A control experiment in the absence of NH_3/NH_4^+, UV light, and TNTs was also carried out to examine the leakage of this closed system. A negligible increase in the peak area was observed after the vial was placed at an ambient atmosphere for 6 h, suggesting the closed system was gastight.

2.5. Characterization of unamended and platinized TNTs

UV–vis spectra of catalysts were obtained using a spectrophotometer (Shimadzu UV-2401 PC) equipped with a diffuse reflectance accessory. Phase identifications of catalysts were conducted by XRD equipped with Cu $K\alpha_1$ radiation (MAC Sience-MXP18) operating under a voltage of 40 kV and a current of 30 mA. The patterns were recorded from 5° to 65° with a scan rate of 2° min^{-1}. The atomic compositions of catalysts were determined by XPS (Kratos Axis Ultra DLD) using the Mg Kα as the excitation source. All binding energies were referenced to the C1s peak at 284.6 eV. The resulting spectra were fitted by XPSPEAK with a linear background and 80% Gausssian/20% Lorentzian peak shape. The Zeta potentials of platinized TNTs at pH = 10 ± 0.2 were measured by Malvern Zetasizer 3000. The field-emission scanning electron microscope (FE-SEM) and high-resolution transmission electron microscope (HRTEM; FEI Tecnai G2; JEOL JEM-3000F) were used to examine the morphology of platinized TNTs. The structure of platinized TNTs demonstrated in the manuscript was constructed by the Ca.R.Ine version 3.1 crystallography package program.

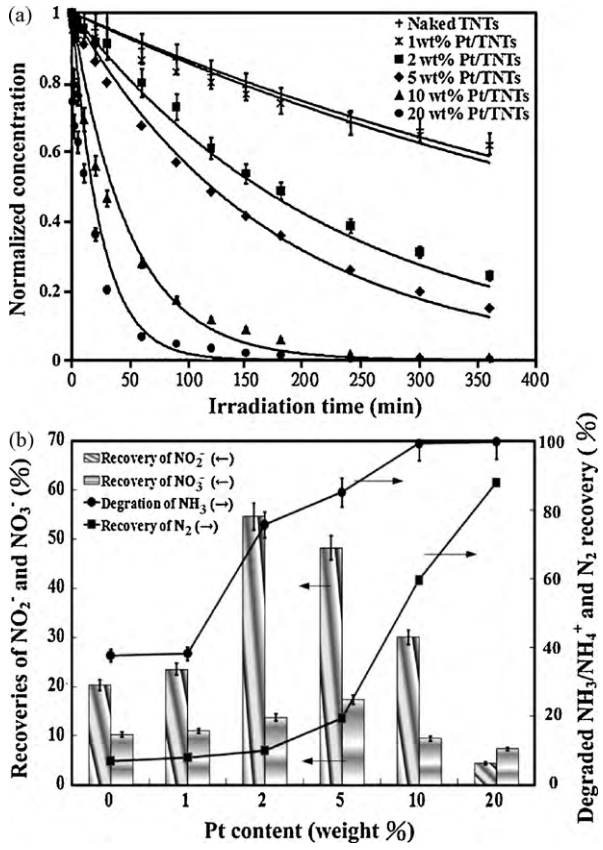

Fig. 1. (a) Time-dependence normalized concentration of NH_3/NH_4^+ as a function of the Pt loading level. (b) Effects of Pt loading on the NH_3/NH_4^+ degradation, N_2, NO_2^-, and NO_3^- recoveries. (NO_2^-/NO_3^- recovery (%) = $[NO_2^-]_{6h}$, $[NO_3^-]_{6h}/[NH_3]_{ini} \times 100$; N_2 recovery (%) = $([NH_3]_{ini}-[NH_3]_{6h}-[NO_2^-]_{6h}-[NO_3^-]_{6h})/[NH_3]_{ini} \times 100$; error bars represent one standard deviation from the replicate analyses).

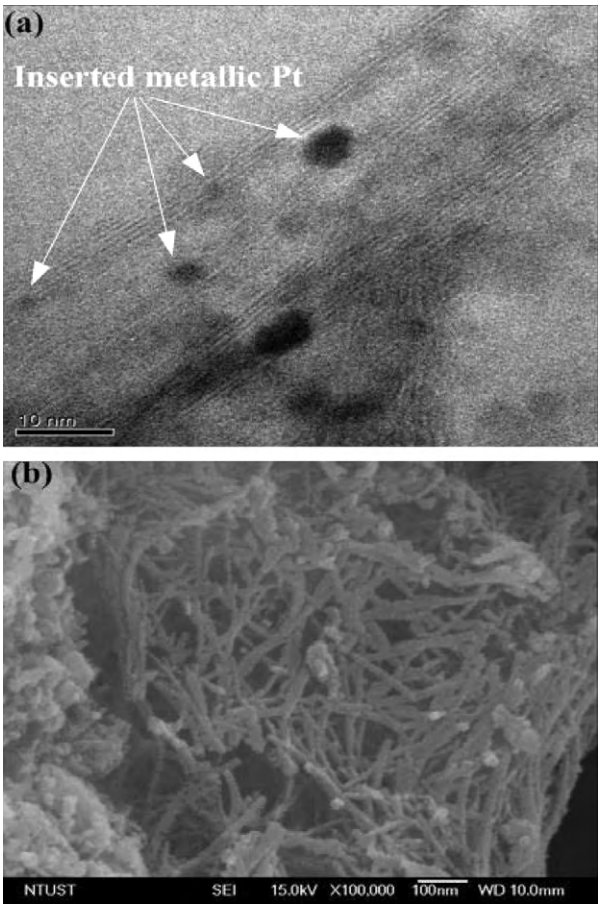

Fig. 2. The morphology of 20 wt% Pt/TNTs observed by (a) HRTEM and (b) FE-SEM.

3. Results and discussion

3.1. Photocatalytic oxidation of NH_3/NH_4^+ over platinized TNTs

3.1.1. Effect of Pt loading on the NH_3/NH_4^+ photooxidation

The time-dependent NH_3/NH_4^+ degradation on the relative Pt loading is illustrated in Fig. 1a. It is clear that the platinized TNTs are more active than unamended TNTs for NH_3/NH_4^+ oxidation. The oxidation rate of NH_3/NH_4^+ enhances with increasing Pt loading. Interestingly, there appeared to be no light-shielding effect as a function of Pt loading up to 20 wt%. In most cases, the photocatalytic performance is inhibited for platinized TiO_2 as the Pt loading is over an optimal amount [2,8]. An optimal Pt loading was found at 0.8 wt%/P25 TiO_2 for NH_3/NH_4^+ oxidation (data not shown). In a related study, Nemoto et al. [8] showed that N_2/H_2 production via NH_3/NH_4^+ photooxidation over platinized TiO_2 reached a maximum at 0.5 wt% Pt/TiO_2. They explained this phenomenon in terms of the light-shielding effect owing to the black-colored Pt loaded on TiO_2. Pretzler et al. also reported that the excess Pt loadings (0.4–5.1 wt%) caused a decrease in the oxidation rate of NH_3/NH_4^+ [2]. However, the light-shielding effect was not apparent for platinized TNTs, which can be explained by the fact that some of the Pt was deposited on the internal surface of TNTs (Fig. 2a). This phenomenon indicates that the incident UV light appears not to be blocked by the internally deposited Pt. Meanwhile, no obvious spherical Pt deposit was observed by SEM (Fig. 2b), which is also indicative of the insertion of Pt into tube structure. This result appears to be corresponding to the study of Bavykin et al. [29] that there was no significant loss of specific activity as Ru(III) loading on TNTs exceeded the optimal level. The phenomenon of Pt insertion into TNTs has also been observed by Ma et al. [22] and Eder et al. [26]. On the other hand, Li et al. [23] have demonstrated that the apparent improvements in photocatalytic activity for Pt-inserted TNTs can be attributed to the enhanced light absorption in the visible region. We have also observed that platinized TNTs show a broadband light absorption in the visible range (Fig. 3a).

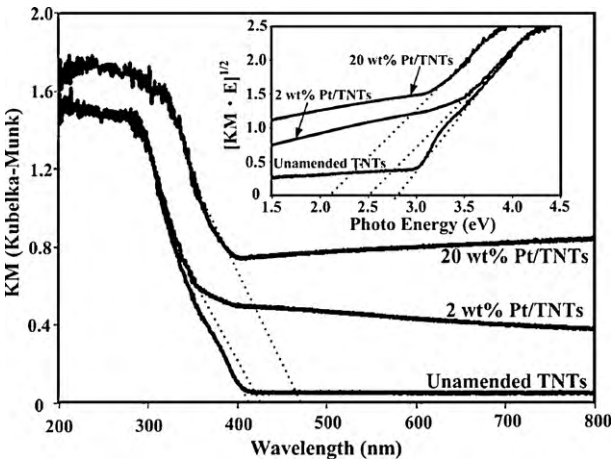

Fig. 3. Diffuse reflection UV–vis spectra of unamended TNTs, 2 wt% Pt/TNTs, and 20 wt% Pt/TNTs (The insert shows the corresponding plots of the Kubelk–Munk (KM) function versus photo energy (E) for the spectra of unamended TNTs, 2 wt% Pt/TNTs, and 20 wt% Pt/TNTs).

Table 1
Rate constants, N_2 selectivity, and Zeta potential for photocatalytic oxidation of NH_3/NH_4^+ over platinized TNTs with different Pt loadings (uncertainties, 95% confidence intervals).

Catalysts	Zeta potentials at pH = 10 ± 0.2 (mV)	$k_{obs} \times 10^3$ (min^{-1})	$k_1 \times 10^3$ (min^{-1})	$k_2 \times 10^3$ (min^{-1})	$k_3 \times 10^3$ (min^{-1})[a]	N_2 selectivity (%)[b]
1 wt% Pt/TNTs	−45.72	1.20	1.16 ± 0.74	2.88 ± 0.83	0.043	3.6
2 wt% Pt/TNTs	−45.90	3.32	2.48 ± 0.45	1.26 ± 0.37	0.84	2.0
5 wt% Pt/TNTs	−44.15	5.30	3.05 ± 0.21	1.22 ± 0.28	2.25	37.7
10 wt% Pt/TNTs	−40.41	14.14	3.42 ± 0.37	4.30 ± 0.33	10.72	75.8
20 wt% Pt/TNTs	−37.00	16.94	2.12 ± 0.45	14.12 ± 0.71	14.82	87.5

[a] k_3 was calculated as the difference between k_{obs} and k_1.
[b] The selectivity to N_2 is defined as the ratio of k_3 to ($k_1 + k_3$).

The observed bathochromic shift as a function of Pt loading can be attributed to the charge-transfer transition between the electrons within Pt ion and the conduction band or valence band of TNTs.

Rapid decreases in the NH_4^+ concentration were also observed in the first 30 s of photocatalysis as shown in Fig. 1a. For example, the normalized concentration of NH_3/NH_4^+ decreased to 0.74 for 20 wt% Pt/TNTs while for unamended TNTs the decrease was only 0.04. The capability of TNTs toward NH_3/NH_4^+ adsorption is clearly enhanced by the platinization of TNTs. This result appears not to be owing to the electrostatic attraction between platinized TNTs and NH_3/NH_4^+ since the Zeta potential of platinized TNTs (negatively charged) increases with increasing loading amount of Pt (Table 1). Instead, Pt itself has been reported to have a relatively strong adsorption affinity for NH_3/NH_4^+ [1,30]. This specific feature is believed to enhance the diffusion of NH_3/NH_4^+ to catalyst surface, a rate-determining step during NH_3/NH_4^+ photooxidation for the case of TiO_2 [5]. The selective formation of N_2 during NH_3/NH_4^+ photooxidation is likely enhanced as well, since the specific adsorption of precursors (NH_3 and NH_x) on Pt deposits is prerequisite for N_2 formation [1,30].

3.1.2. Determination of N_2 over platinized TNTs

The photocatalytic oxidation of NH_3/NH_4^+ over TiO_2 in an oxygen-saturated atmosphere yields NO_2^- and NO_3^- along with N_2 and trace amounts of N_2O [1–7]. N_2 was supposed to be the dominant gaseous product in our study, since the yield of N_2O was previously reported to be far smaller than that of N_2 [1,2]. N_2 measurements were carried out in a closed system in which 5 mg of the catalyst (i.e., the loading concentration is the same as that in the above photocatalytic experiments) along with 10 mL of 20 mg-N/L NH_3/NH_4^+ solution was introduced into a 15 mL quartz bottle which was then exposed to UV light. No N_2 was detected in the case of unamended TNTs whereas the amount of N_2 produced for 2 and 20 wt% Pt/TNTs was obtained in 11.3 and 57.9 μg, respectively (Table 2). The direct quantitative measurement of the produced N_2 was in good agreement with the total nitrogen mass balance (error < 5%) (Table 2). Therefore, the produced N_2 can be reasonably estimated from the N-mass deficits, since NO_2^-, NO_3^-, and NH_3/NH_4^+ were readily detected in the aqueous solution.

3.1.3. Effect of Pt loading on the recoveries of NO_2^-, NO_3^- and N_2

Fig. 1b shows the recoveries of NO_2^-, NO_3^-, and N_2 after 6 h NH_3/NH_4^+ photooxidation. Even though there appeared to be no noticeable difference in the extent of NH_3/NH_4^+ oxidation between unamended TNTs and 1 wt% Pt/TNTs (Fig. 1a), the increase in the recoveries of NO_2^-/NO_3^- suggests that the improved photocatalytic activity is due to the platinization of TNTs (Fig. 1b). The recoveries of NO_2^-/NO_3^- reached maximum at Pt loadings of 2 and 5 wt%, followed by a drop with a further increase in the Pt loading. This indicates that the oxidation of NH_3/NH_4^+ to NO_2^- is sensitive to an optimal Pt loading level. However, the effect of Pt loading on N_2 recovery did not follow the same trend as the recoveries of NO_2^-/NO_3^-. It is clear that increasing Pt loading favors the photoconversion of NH_3/NH_4^+ into N_2 rather than NO_2^-/NO_3^-. Similar results were reported by Lee et al. [1] and interpreted in terms of NH_3 adsorbed on the metallic Pt ($NH_{3(ad,\,Pt)}$) as a prerequisite step leading to N_2 formation. In contrast, NO_2^- is formed primarily from NH_3 adsorbed on the non-platinized TNT sites ($NH_{3(ad,\,TNTs)}$).

Regarding the possible pathway of N_2 formation, N_2 can be formed either by the oxidation of NH_3/NH_4^+ or by the reduction of NO_2^-/NO_3^-. Photocatalysis of NO_2^-, therefore, was carried out in order to determine the extent of N_2 formation from the photocatalytic reduction of NO_2^-. However, after 6 h photoirradiation, NO_3^- was the only observed product over platinized TNTs with N-mass recoveries for 2% and 20% Pt/TNTs of 99.0% and 102.7%, respectively (Table 3). Thus, the N_2 formation during photocatalytic oxidation of NH_3/NH_4^+ is exclusively from the selective oxidation of NH_3/NH_4^+. A kinetic equation with parallel and consecutive reactions is expressed to describe the kinetics of NH_3/NH_4^+ photooxidation over platinized TNTs, as shown in Scheme 1.

3.1.4. Kinetics and N_2 selectivity of NH_3/NH_4^+ photooxidation reaction over platinized TNTs

Scheme 1 illustrates a sequence of reactions for the photooxidation of total ammonia where k_1, k_2, and k_3 are the pseudo first-order rate constants of conversion of NH_3/NH_4^+ into NO_2^-, conversion of NO_2^- into NO_3^-, and conversion of NH_3/NH_4^+ into N_2, respectively. The values of k_1 and k_2 were determined by a least-square fitting of kinetic data for NO_2^- formation, while k_3 was obtained from the difference between k_1 and k_{obs} of NH_3/NH_4^+ photooxidation.

Table 2
Determination of N_2 produced over unamended, 2 wt% Pt/TNTs, and 20 wt% Pt/TNTs.

Catalysts	Degraded NH_3-N (%)[a]	Recovery of NO_2^--N (%)[b]	Recovery of NO_3^--N(%)[c]	Mass recovery as N atom (%)[d]	N_2 mass (μg)[e]	N_2 mass (μg)[f]
Unamended TNTs	10.0	9.2	0.0	99.2	1.6	N.D.[g]
2 wt% Pt/TNTs	13.5	5.1	2.3	93.9	12.2	11.3
20 wt% Pt/TNTs	40.0	7.1	4.1	71.2	57.6	57.9

[a] $([NH_3]_{ini} - [NH_3]_{6\,h}) \times 100/[NH_3]_{ini}$.
[b] $[NO_2^-]_{6\,h} \times 100/[NH_3]_{ini}$.
[c] $[NO_3^-]_{6\,h} \times 100/[NH_3]_{ini}$.
[d] $(14/46[NO_2^-]_{6\,h} + 14/62[NO_3^-]_{6\,h} + 14/17[NH_3]_{6\,h}) \times 100/14/17[NH_3]_{ini}$.
[e] The mass of N_2 is calculated from the N-mass deficits.
[f] The mass of N_2 is determined by GC/TCD.
[g] Not determined.

Table 3
Degraded NO_2^-, NO_3^- recovery, mass recoveries as N atom and observed rate constant for NO_2^- degradation over 2% and 20 wt% Pt/TNTs after 6 h NH_3/NH_4^+ photooxidation.

Catalysts	Degraded NO_2^--N (%)[a]	Recovery of NO_3^--N (%)[b]	Recovery of NH_3/NH_4^+-N (%)	Mass recovery as N atom (%)[c]	$k_{obs} \times 10^3$ (min^{-1})
2 wt% Pt/TNTs	55.5	54.6	N.D.	99.0	2.3
20 wt% Pt/TNTs	79.7	82.4	N.D.	102.7	4.6

[a] $([NO_2^-]_{ini} - [NO_2^-]_{6h}) \times 100/[NO_2^-]_{ini}$.
[b] $[NO_3^-]_{6h} \times 100/[NO_2^-]_{ini}$.
[c] $(14/46[NO_2^-]_{6h} + 14/62[NO_3^-]_{6h}) \times 100/14/46[NO_2^-]_{ini}$.

$$>TiOH \rightleftharpoons >TiO^- + H^+ \ (h\nu \geqq 254 \text{ nm at solution pH of 10})$$

$$TiO^- + NH_3 \longrightarrow TiO^-{:}NH_3 \xrightarrow[O_2]{k_1} TiOH^- + NO_2^- + H_2O \xrightarrow[\frac{1}{2}O_2]{k_2} TiOH^- + NO_3^- + H_2O$$

$$Pt(TNTs) + 2NH_3 \longrightarrow H_3N{:}Pt(TNTs){:}\ NH_3 \xrightarrow[\frac{3}{2}O_2]{k_3} N_2 + Pt(TNTs) + 3H_2O$$

Scheme 1. A simplified mechanism including parallel and consecutive reactions for the photocatalytic oxidation of NH_3/NH_4^+ over platinized TNTs.

The effect of Pt on the value of k_1 is shown in Table 1. A two-fold increase in k_1 was observed as the Pt loading was increased from 1 to 2 wt%, which was followed by a gradual increase in k_1 over the Pt loadings from 2 to 10 wt%. However, additional Pt loading up to 20 wt% resulted in a dramatic decline in k_1. This is consistent with the observed trend in the recovery of NO_2^- as shown in Fig. 1b. The initial increase in k_1 can be attributed to the enhanced production of hydroxyl radical, OH•, due to more efficient electron–hole separation in the presence of Pt. Further increase in Pt loading invariably decreases the amount of $NH_{3(ad,\ TNTs)}$, and thus to a decline of k_1 since the increasing $NH_{3(ad,\ Pt)}$ amount dominates over $NH_{3(ad,\ TNTs)}$ for the competition of OH•. The significant decrease in k_1 at a loading of 20 wt% Pt is due to the overwhelming amount of $NH_{3(ad,\ Pt)}$ versus $NH_{3(ad,\ TNTs)}$. This factor accounts for a substantial enhancement in the N_2 selectivity as well.

The relative effect of Pt loading on k_2 is summarized in Table 1. k_2 is low at lower Pt loadings and then increases at higher loadings (>10 wt%). For the case of 1–5 wt% Pt loadings, a decrease in k_2 is consistent with a increasing k_1 and with the net accumulation of NO_2^-. A substantial increase in k_2 for the Pt loadings from 10–20 wt% can be explained by the Zeta potential which suggests a decrease in the number of TiO^- site (Table 1). In other words, the decline of electrostatic repulsion between NO_2^- and negatively charged platinized TNTs lead to an increase in k_2. Furthermore, the k_{obs} of NO_2^- oxidation is one order of magnitude less than that of NH_3/NH_4^+ in the case of 20 wt% Pt/TNTs (Tables 1 and 3). Lower activity for NO_2^- oxidation versus NH_3/NH_4^+ oxidation is most likely due to the relatively high electrostatic repulsion.

The ratio of k_3 to k_{obs} (i.e. $k_3/(k_1 + k_3)$) can be utilized as a measure of N_2 selectivity, since the relative magnitude of this ratio is indicative of the NH_3/NH_4^+ oxidation branching ratio [2]. As demonstrated in Table 1, N_2 selectivity is increased as the Pt loading is increased. Lee et al. [1] reported the conversion efficiency at 65–70% for NH_3 going to N_2 over platinized TiO_2 in an air-saturated atmosphere. In our case, 95% of NH_3/NH_4^+ was oxidized within 1 h with less than 10% of the total NH_3 selectively transformed into NO_2^-/NO_3^-. This result again argues for an enhanced N_2 selectivity obtained with platinized TNTs.

3.2. Characterizations of unamended and platinized TNTs

3.2.1. UV–vis DRS for platinized TNTs

As mentioned above, platinized TNTs give a broader band absorption throughout the visible portion of the spectrum (Fig. 3); this can be ascribed to the darker grey color of platinized TNTs. Tauc plots [31] were used to determine the apparent band gaps of catalysts (the insert in Fig. 3). Extrapolation of these lines to the photon energy yields the band gaps at 2.79, 2.54, and 2.12 eV for unamended TNTs, 2 and 20 wt% Pt/TNT, respectively. This observation clearly indicates that the presence of Pt results in the formation of additional energy levels above the valence band of unamended TNTs. As expected, the narrowest band gap was found for 20 wt% Pt/TNTs, which corresponds to the highest photoactivity for NH_3/NH_4^+ oxidation due to the more intense broadband absorption in the visible light.

3.2.2. XRD patterns for TNTs before and after NH_3/NH_4^+ oxidation

Unamended TNTs is assigned to $Na_xH_{2-x}Ti_3O_7$ based on the observed XRD patterns. This assignment is consistent with the results demonstrated in the previous studies [16,17]. Neither the position nor the sharp of the diffraction peaks were changed for TNTs after NH_3/NH_4^+ photooxidation; this suggests that there was no distortion of the TNT structure during the course of the photocatalytic reaction. In the case of platinized TNTs, the titanate phase dominated at 2 wt% Pt/TNTs, while the discrete anatase phase, along with Pt, and PtO_2 were evident in the case of 20 wt% Pt/TNTs (Fig. 4). The high Pt loading appears to favor the transformation of the titanate phase into the anatase phase with retention of the tubular structure. Furthermore, PtO_2 coexists with the metallic Pt in each case of the platinized TNTs. Pretzer et al. [2] reported that the oxidation rate and selectivity of titania-catalyzed NH_3/NH_4^+ oxidation

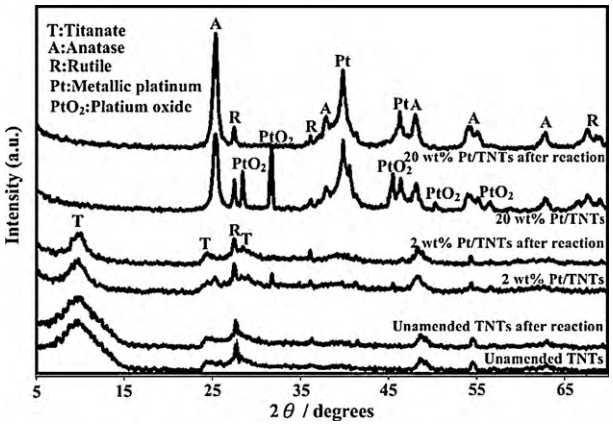

Fig. 4. XRD patterns of unamended TNTs, 2 wt% Pt/TNTs, and 20 wt% Pt/TNTs before and after the reaction of NH_3/NH_4^+ photocatalysis.

was retarded in the presence of PtO_2 due to its inability to stabilize intermediate NH_x species and to its impact as a recombination center for electron–hole pairs. In contrast, PtO_2 supported on platinized TNTs presented no negative effect on the performance of NH_3/NH_4^+ photooxidation.

The XRD patterns of platinized TNTs changed somewhat after the NH_3/NH_4^+ photooxidation (Fig. 4). In the specific case of the 2 or 20 wt% Pt/TNTs, the PtO_2 peak was absent. This result can be ascribed to the photoreduction of PtO_2 to metallic Pt, which is consistent with XPS analysis demonstrated in the following section. The reduction of PtO_2 may occur by either direct reaction with NH_3/NH_4^+ (as an electron donor) or by capture of conduction band electrons. To clarify the role of PtO_2 during NH_3/NH_4^+ oxidation, a control experiment was carried out with PtO_2 as the only metal oxide in the absence of light. NH_3/NH_4^+ was not oxidized, which implies that the reduction of PtO_2 into Pt occurs exclusively due to photoreduction by conduction band electrons.

3.2.3. XPS spectra of platinized TNTs after NH_3/NH_4^+ oxidation

In the case of 2 wt% Pt/TNTs, the peaks occurring at 71.0 and 74.3 eV in the Pt ($4f_{7/2,5/2}$) spectrum are assigned to the metallic Pt whereas the Pt ($4f_{7/2,5/2}$) spectra of 20 wt% Pt/TNTs consists of broad peaks characteristic of two oxidation states. The spectra can be deconvoluted into two doublets in which 71.0 (74.3 eV) and 73.7 eV (76.8 eV) are assigned to metallic Pt and PtO_2, respectively. These observations are consistent with the observed XRD patterns in that Pt and PtO_2 coexist in the 20 wt% Pt/TNTs. For 2 wt% Pt/TNTs after NH_3/NH_4^+ photooxidation, the spectra of Pt4f consist of metallic Pt (88.6%) and smaller fraction of oxidized Pt (Pt_{ox}) (11.4%) that dispersed over TNTs (Fig. 5a). The same result was observed in the case of 20 wt% Pt/TNTs after NH_3/NH_4^+ photooxidation that the relative portion of Pt_{ox} increases at the expense of the metallic Pt. Pt_{ox} was reported to be generated as a result of the chemisorb oxygen on a clean Pt surface under ambient conditions during photolysis [32]. The presence of Pt_{ox} in platinized TNTs after reaction can be attributed to the high degree of dispersion of Pt on the TNT surface [32]. Meanwhile, XPS analysis showed no PtO_2 on platinized TNTs after NH_3/NH_4^+ photocatalysis, which is consistent with the observed XRD patterns (i.e., PtO_2 is eliminated via reduction by conduction band electrons). In addition, there is a substantial decrease in the binding energy of metallic Pt from 71.2 to 69.4 eV, which is indicative of change in the structural environment within platinized TNTs. The shift to the lower binding energy can be explained in terms of the presence of Pt_{ox}, which should yield an increase in the electron charge density of the metallic Pt.

With respect to the N 1s spectra, four peaks are observed at 404.4, 401.6, 399.0, and 397.4 eV in the case of unamended TNTs after reaction (Fig. 5b). The four peaks are assigned in order as N–Na, NH_4^+, NH_3, and N–Ti, respectively [17,33–36]. The formation of N–Na and N–Ti is indicative of the intercalation of NH_3/NH_4^+ into TNT structure, whereas the protonation of NH_3 is due to the BrØnsted acidity of the unamended TNTs [17]. In contrast, only NH_3 was detected in the N 1s region of 2 wt% Pt/TNTs after reaction. This suggests that the Pt deposits suppress the intercalation of NH_3/NH_4^+ into the structure of TNTs during NH_3/NH_4^+ photooxidation. Moreover, no obvious peak emerges in the case of 20 wt% Pt/TNTs after reaction, which indicates that a negligible amount of N remains on the surface of the catalyst. The atomic concentration of N species for unamended TNTs, 2 wt% Pt/TNTs, and 20 wt% Pt/TNTs after reaction are 1.69%, 1.24% and 0.11%, respectively. The adsorbed N species on unamended or platinized TNTs should not be due to NO_2^-/NO_3^- because of the electrostatic repulsion between NO_2^-/NO_3^- and negatively charged TNTs in the suspension with pH at 10. Therefore, the residual N species on the surface of unamended and platinized TNTs are exclusively due to the contribution of NH_3/NH_4^+. This result in consistent with the observation that platinized TNTs favor the transformation of NH_3 in N_2, since negligible amounts of N-species were detected.

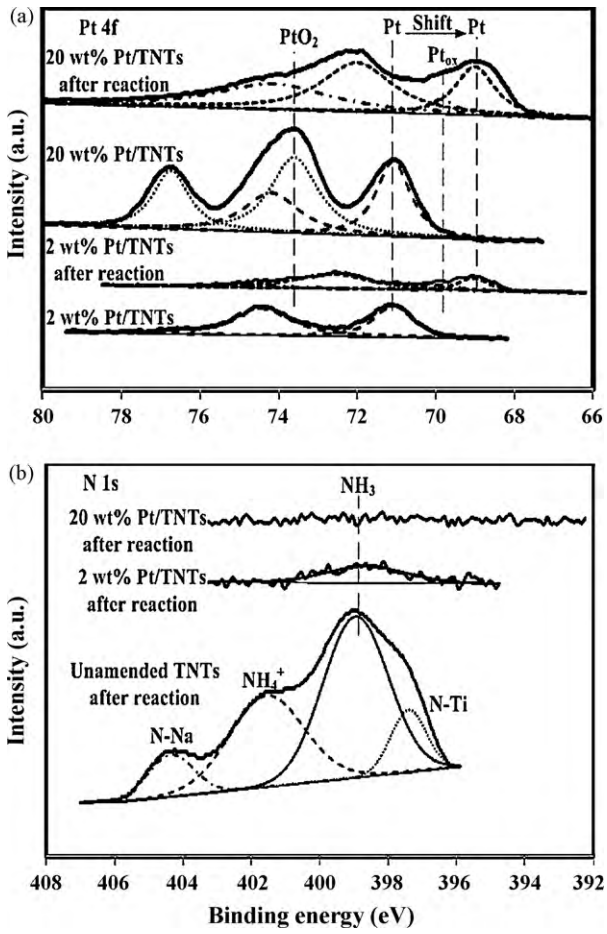

Fig. 5. XPS analysis for (a) Pt 4f region of unamended TNTs and platinized TNTs before and after reaction. (b) N 1s region of unamended TNTs, 2 wt% Pt/TNTs, and 20 wt% Pt/TNTs after reaction.

3.3. Mechanism and reaction pathway of NH_3/NH_4^+ photooxidation over platinized TNTs

Based on our results and the previous findings [1,2,37,38], the suggested mechanism and conceptual reaction pathway for NH_3/NH_4^+ photooxidation over platinized TNTs are illustrated in Scheme 2. As demonstrated, charge pairs generate as TNTs is illuminated by UV light (Reaction (1)). The resulting valence-band holes, h^+, and conduction-band electrons, e^-, can be consumed in the catalyzed oxidation and reduction, respectively. For example, the valence-band holes will oxidized surface hydroxyl groups to surface hydroxyl radicals. On the other hand, the conduction band electrons are trapped on the titanate surface as Ti(III) (reaction (2)) or on Pt/PtO_2 (reaction (3)). Meanwhile, the migration rate of NH_3/NH_4^+ to platinized TNTs is enhanced with increasing electrostatic attraction between NH_3/NH_4^+ and negatively charged TNTs, after which NH_3 is adsorbed either on the Pt deposits or on the titanate sites. The NH_3 adsorbed on Pt deposits is transformed into $^\bullet NH_2$ which is a prerequisite species to the formation of N_2 (Eq. (4)). In comparison, the NH_3 adsorbed on titanate reacts with hydroxyl radicals to form NH_2OH which is an intermediate to form NO_2^-. Further oxidation of NO_2^- will lead to the formation of NO_3^- (Eq. (5)).

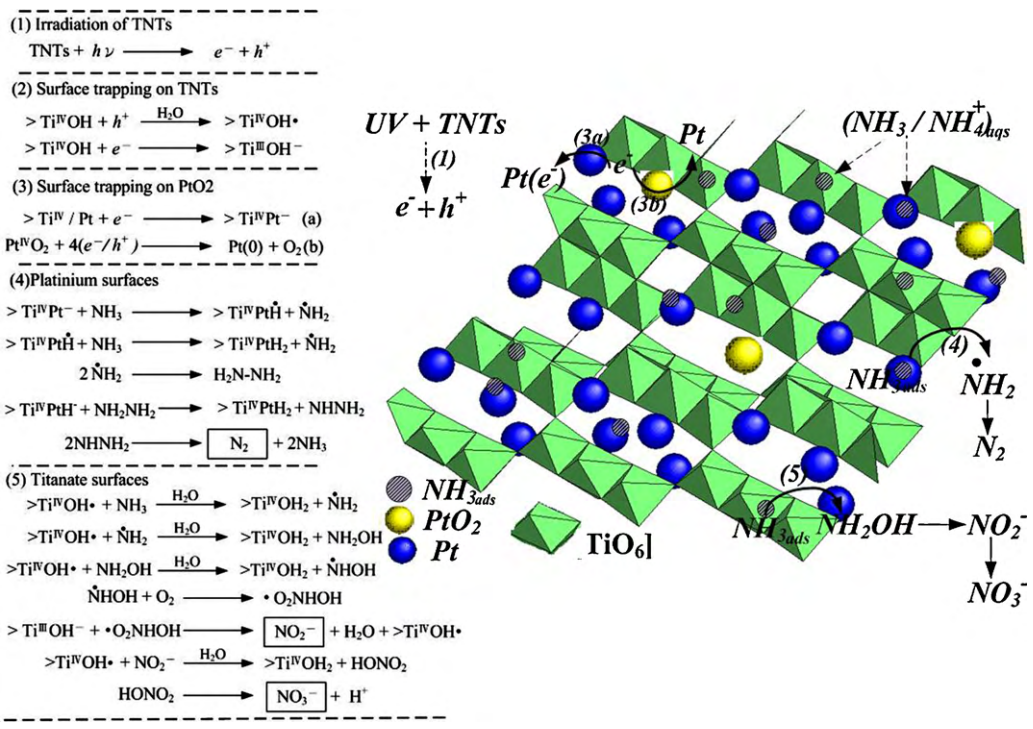

Scheme 2. Mechanism and reaction pathway for photocatalytic oxidation of NH_3/NH_4^+ over platinized TNTs.

4. Conclusions

The photocatalytic oxidation of NH_3/NH_4^+ over platinized TNTs can be considered as a candidate treatment process for denitrification. Owing to the ion exchange property, TNTs can accommodate a high Pt loading which is advantageous to the selective formation of N_2 during NH_3/NH_4^+ photooxidation. Furthermore, there is no UV light-shielding effect for platinized TNTs since Pt is primarily deposited on the internal surface of the TNTs as opposed to being on the external surface of the TNTs.

Acknowledgment

The authors gratefully acknowledge the funding from the National Science Council of Taiwan (NSC 95-2221-E-002-143-MY3).

References

[1] J. Lee, H. Park, W. Choi, Environ. Sci. Technol 36 (2002) 5462–5468.
[2] L.A. Pretzer, P.J. Carlson, J.E. Boyd, J. Photochem. Photobiol. A: Chem. 200 (2008) 246–253.
[3] C.H. Pollema, E.B. Milosavljevic, J.L. Hendrix, L. Solujic, J.H. Nelson, Monatsh. Chem. 123 (1992) 333–339.
[4] A. Wang, J.G. Edwards, J.A. Davies, Sol. Energy 52 (1994) 459–466.
[5] X. Zhu, S.R. Castleberry, M.A. Nanny, E.C. Butler, Environ. Sci. Technol. 39 (2005) 3784–3791.
[6] E.M. Bonsen, S.S. Schroeter, H. Jacobs, J.A.C. Broekaert, Chemosphere 35 (1997) 1431–1445.
[7] A. Bravo, J. Garcia, X. Domènech, J. Peral, J. Chem. Res. (1993) 376–377.
[8] J. Nemoto, N. Gokan, H. Ueno, M. Kaneko, J. Photochem. Photobiol. A: Chem. 185 (2007) 295–300.
[9] J. Taguchi, T. Okuhara, Appl. Catal. A: Gen. 194–195 (2000) 89–97.
[10] T. Kasuga, M. Hiramatsu, A. Hoson, T. Sekino, K. Niihara, Lanngmuir 14 (1998) 3160–3163.
[11] T. Kasuga, M. Hiramatsu, A. Hoson, T. Sekino, K. Niihara, Adv. Mater. 11 (1999) 1307–1311.
[12] A. Nakahira, W. Kato, M. Tamai, T. Isshiki, K. Nishio, J. Mater. Sci. 39 (2004) 4239–4245.
[13] C.C. Tsai, H. Teng, Chem. Mater. 16 (2004) 4352–4358.
[14] V. Štengl, S. Bakardjieva, J. Šubrt, E. Veçerníková, L. Szatmary, M. Klementová, V. Balek, Appl. Catal. B: Environ. 63 (2006) 20–30.
[15] S. Zhang, W. Li, Z. Jin, J. Yang, J. Zhang, Z. Du, Z. Zhang, J. Solid State Chem. 11 (2004) 1365–1371.
[16] H.H. Ou, S.L. Lo, Y.H. Liou, Nanotechnology 18 (2007) 175702–175707.
[17] H.H. Ou, C.H. Liao, Y.H. Liou, J.H. Hong, S.L. Lo, Environ. Sci. Technol. 42 (2008) 4507–4512.
[18] H.H. Ou, S.L. Lo, Sep. Purif. Technol. 58 (2007) 179–191.
[19] K. Nishijima, Y. Fujisawa, N. Murakami, T. Tsubota, T. Ohno, Appl. Catal. B: Environ. 84 (2008) 584–590.
[20] K. Nishijima, Y. Fujisawa, T. Tsubota, T. Ohno, Appl. Catal. B: Environ. 92 (2009) 56–60.
[21] N. Bouazza, M. Ouzzine, M.A. Lillo-Ródenas, D. Eder, A. Linares-Solano, Appl. Catal. B: Environ. 92 (2009) 377–383.
[22] X. Ma, C. Feng, Z. Jin, J. Yang, Z. Zhang, J. Nanopart. Res. 7 (2005) 281–283.
[23] H.L. Li, W.L. Luo, W.Y. Tian, T. Chen, C. Li, M. Sun, D. Zhu, R.R. Liu, Y.L. Zhao, C.L. Liu, Spectrosc. Spect. Anal. 29 (2009) 1623–1626 (in Chinese).
[24] K.P. Yu, W.Y. Yu, M.C. Kuo, Y.C. Liou, S.H. Chien, Appl. Catal. B: Environ. 84 (2008) 112–118.
[25] Y. Sato, M. Koizumi, T. Miyao, S. Nait, Catal. Today 111 (2006) 164–170.
[26] D. Eder, M.S. Motta, I.A. Kinloch, A.H. Windle, Phys. E 37 (2007) 245–249.
[27] C.H. Lin, C.H. Lee, J.H. Chao, C.Y. Kuo, Y.C. Cheng, W.N. Huang, Y.M. Hunag, M.K. Shih, Catal. Lett. 98 (2004) 61–66.
[28] D.V. Bavykin, A.A. Lapkin, P.K. Plucinski, L. Torrente-Murciano, J.M. Friedrich, F.C. Walsh, Top. Catal. 39 (2006) 151–160.
[29] D.V. Bavykin, A.A. Lapkin, P.K. Plucinski, J.M. Friedrich, F.C. Walsh, J. Catal. 235 (2005) 10–17.
[30] A.C.A. de Vooys, M.T.M. Koper, R.A. van Santen, J.A.R. van Veen, J. Electroanal. Chem. 506 (2001) 127–137.
[31] J. Tauc, R. Grigorvici, A. Vancu, Phys. Status Solid 15 (1996) 627–637.
[32] C. Millon, D. Riassetto, G. Berthome, F. Roussel, M. Langlet, J. Photochem. Photobiol. A: Chem. 189 (2007) 344–348.
[33] K. Burger, F. Tschismarov, H. Ebel, J. Electron Spectrosc. Relat. Phenom. 101 (1977) 461–465.
[34] M. Datta, H.J. Mathieu, D. Landolt, Appl. Surf. Sci. 18 (1984) 299–314.
[35] D.N. Hendrickson, J.M. Hollander, W.L. Jolly, Inorg. Chem. 8 (1969) 2642–2648.
[36] M. Sathish, B. Viswanathan, R.P. Viswanath, Appl. Catal. B 74 (2007) 307–312.
[37] H. Gerischer, A. Mauerer, J. Electroanal. Chem. 25 (1970) 421–433.
[38] M.A. Ferguson, M.R. Hoffmann, J.G. Hering, Environ. Sci. Technol. 39 (2005) 1880–1886.